Physica **106A** (1981) 226–238 © *North-Holland Publishing Co.*

PHASE DIAGRAM OF THE TWO-DIMENSIONAL LENNARD-JONES SYSTEM; EVIDENCE FOR FIRST-ORDER TRANSITIONS

J.A. BARKER, D. HENDERSON and F.F. ABRAHAM

IBM Research Laboratory, San Jose, California 95193, USA

Abstract

There has recently been extensive interest in the nature of the melting/freezing transition for a two-dimensional system of molecules interacting with Lennard-Jones 6:12 potentials, which is a prototype for physisorbed systems. We have therefore made a detailed study of the thermodynamics of the phase diagram for this system. We first made calculations using liquid-state perturbation theory for the fluid state and a self-consistent cell theory for the solid state to determine thermodynamic functions; these results led to ordinary first-order phase transitions between solid/fluid and liquid/gas phases, in agreement with the constant-pressure Monte Carlo results of Abraham. We refined the calculations by using constant-pressure and constant-density Monte Carlo results to improve the accuracy of the calculated free energies, and we determined the two-phase equilibria by making direct Monte Carlo calculations for two-phase systems. The results are internally consistent and lead to a phase diagram qualitatively similar to the three-dimensional Lennard-Jones system.

Résumé

La nature de la transition fusion/solidification pour un système bidimensionel de molécules avec des interactions représentées par des potentiels Lennard-Jones 6:12, qui constitue un prototype des systèmes physisorbés, a suscité récemment beaucoup d'intérêt. C'est pourquoi nous avons fait une étude détaillée de la thermodynamique du diagramme des phases pour ce système. Nous avons d'abord fait des calculs, en utilisant la théorie des perturbations de l'état liquide dans le cas de l'état fluide, et une théorie cellulaire self-consistante dans le cas de l'état solide, pour déterminer les fonctions thermodynamiques; ces résultats ont conduit à des transitions de phase ordinaires du premier ordre entre les phases solide/fluide et liquide/gaz, en accord avec les résultats Monte Carlo à pression constante de Abraham. Nous avons raffiné les calculs en utilisant des résultats Monte Carlo à pression constante et à densité constante pour améliorer la précision des énergies libres calculées, et nous avons déterminé les équilibres à deux phases en faisant des calculs Monte Carlo directs pour les systèmes à deux phases. Les résultats sont cohérents et conduisent à un diagramme des phases qualitativement semblable à celui du système Lennard-Jones tridimensionnel.

1. Introduction

Recently, there has been considerable interest in the properties of a two-dimensional system of molecules interacting with Lennard-Jones potentials. Computer simulations of this system have been reported by Fehder[1]), Tsien and Valleau[2]), Toxvaerd[3,4]), Henderson[5]), Frenkel and McTague[6]), Abraham[7,8]), and van Swol et al.[9]).

One reason for this interest is the fact that the two-dimensional Lennard-Jones fluid is a prototype for physisorbed gases, where effects of gas–substrate interactions may be treated by a perturbation expansion. A second reason for this interest is the recent theory of Halperin and Nelson[10,11]) for the melting of two-dimensional solids. According to this theory, as the temperature is increased melting proceeds via two second-order phase transitions. At first, there is a transition from the solid phase to an orientationally ordered, but translationally disordered, phase, called the hexatic phase. At a higher temperature the hexatic phase undergoes another second-order transition to an isotropic fluid phase.

Direct support for the Halperin–Nelson theory is provided by the computer simulations in a constant density and energy ensemble of Frenkel and McTague[6]) who claimed to observe in a system of two-dimensional Lennard-Jones molecules an orientationally ordered, but translationally disordered, phase bounded by two second-ordered transitions. This observation is at variance with the earlier computer simulations of Alder and Wainwright[12]) for hard disks and Tsien and Valleau[2]) and Toxvaerd[4]) for Lennard-Jones molecules. However, Nelson and Halperin[11]) have speculated that the melting transition could be first-order at high pressures but second-order at low pressures. It has been suggested[6,11]) that the studies of Tsien, Valleau and Toxvaerd examined a high pressure regime where melting becomes first-order.

The most plausible explanation of the observations of Frenkel and McTague is that they did not observe an exotic phase but rather they observed solid–fluid coexistence in a normal first-order phase transition taking place at constant density. Abraham[7]) has demonstrated the validity of this explanation by performing computer simulations in a constant pressure and temperature ensemble where solid–fluid coexistence is not possible. Doing the simulations at both high and low pressures, he concluded that two-dimensional melting is always first-order. The subsequent simulations of Toxvaerd[4]) and Van Swol et al.[8]) have supported this conclusion.

In order to study further the two-dimensional Lennard-Jones system and its transitions, we have calculated the phase diagram of this system by means of Monte Carlo computer simulations in both the constant temperature and density and constant pressure and temperature ensembles. To obtain the phase diagram, we must calculate free energies from the simulations. As will be seen below, this requires considerable computer time. In order to minimize the computer time we first calculated the phase diagram of the Lennard-Jones system using perturbation theory to describe the fluid phase and an approximate self-consistent cell theory to describe the solid phase. As a result we were able to confine our simulations to the relevant parts of the phase diagram.

2. Perturbation theory and self-consistent cell theory

The simplest treatment of the phase transitions of a Lennard-Jones system is that used by Henderson and Barker[13]) in three dimensions. They used the Barker–Henderson perturbation theory[14]) to describe the fluid phases and a simple cell theory to describe the solid phase. We have adapted this procedure for our study of the two-dimensional system.

In the Barker–Henderson perturbation theory the free energy of a fluid is calculated by means of an expansion using the hard-sphere fluid as a reference system. The expansion parameters are the strength of the long-range part of the potential and an inverse steepness parameter for the short-range part of the potential. In three dimensions, this expansion converges very rapidly and is useful even for liquids. In two dimensions, the convergence is slower. In order to describe satisfactorily the two-dimensional liquid, a semi-empirical third-order term must be included[5]).

In our approximate calculation of the free energy of the two-dimensional solid, a self-consistent cell theory[15]), based upon the application of the Bethe approximation to a single-occupancy cell theory, was used. The details of application of this theory to hard spheres and hard discs has been given by Barker and Cowley[16]). The details of its application to Lennard-Jones systems will be given subsequently[17]).

Once the free energies of the solid and fluid phases had been determined, the vapor–liquid and liquid–solid equilibria were calculated by constructing common tangents in a Helmholtz free energy versus volume diagram. The resulting phase diagrams are plotted in figs. 1 and 2 and the resulting critical and triple point constants are given in tables I and II.

3. Monte Carlo calculations

We have performed Monte Carlo simulations using both constant-density and constant-pressure ensembles for a system of 256 particles with periodic boundary conditions. One such calculation for either ensemble gives a single point on the (p, ρ, T) and (U, ρ, T) surfaces (p, ρ, T, U are pressure, density, temperature and internal energy). The primary Monte Carlo results are given in table III. For each calculation we used at least 1.2×10^6 configurations (with acceptance ratio close to 0.5) to calculate averages and 0.35×10^6 configurations to approach equilibrium; in the two-phase region we used several times as many configurations.

To determine the Helmholtz free energy A and chemical potential which are also required for locating phase boundaries we have integrated the

TABLE I
Critical point constants

T_c^*	p_c^*	ρ_c^*	$p_c/\rho_c kT_c$
0.56[a]	0.046	0.325	0.252
0.533[b]	0.037	0.335	0.209

[a] From perturbation theory and cell theory.
[b] From Monte Carlo calculations and virial coefficients.

TABLE II
Triple point constants

T_t^*	p_t^*
0.41[a]	0.006
0.415[b]	0.0056

[a] From perturbation theory and cell theory.
[b] From Monte Carlo calculations.

equations

$$\frac{\partial A^*}{\partial \rho^*} = p^*/\rho^{*2} \tag{1}$$

and

$$\frac{\partial}{\partial T^*}[A^*/T^*] = -U^*/T^{*2} \tag{2}$$

along appropriate reversible paths in the (ρ, T) plane joining reference thermodynamic states for which the free energy is known to the thermodynamic states of interest. In eqs. (1) and (2) $A^* = A/N\epsilon$, $U^* = U/N\epsilon$, $T^* = kT/\epsilon$, $\rho^* = \rho\sigma^2$, and $p^* = p\sigma^2/\epsilon$. For fluid states the most convenient reference state is zero density at a particular temperature which we chose as $T^* = 1.0$. For solid states we chose the reference state $T^* = 0.0$, $\rho^* = 0.9165$. The integration paths which we used are shown in fig. 3. The density $\rho^* = 0.9165$ lies outside the two-phase region for all the temperatures we studied so that there is no problem with reversibility. At our lowest temperature the fluid path lies in the liquid–vapor two-phase region. In this range we imposed a constraint in the manner of Hansen and Verlet[18]) to ensure that phase separation would not occur. Since we used this constraint only in a high density region it should not lead to serious error.

In the neighborhood of $T^* = 0$ the classical solid behaves as a purely harmonic crystal for which the free energy can be calculated by standard methods of lattice dynamics, and this calculation has been performed with high accuracy for the two-dimensional Lennard-Jones solid by Phillips and Bruch[19]); the density $\rho^* = 0.9165$ corresponds to the lattice parameter $L/r_0 = 1.00$ in their paper. From their results we see that the free energy in the neighborhood of $T^* = 0$ is given by

$$A^* = U_0^* + [S_0^* + \ln(2\pi)]T^* - T^* \ln T^* + O(T^{*2}), \tag{3}$$

where U_0^* is reduced static lattice energy and S_0^* is a constant given by the value for $\Lambda^*/T^* = 0$ of $F = [\mathcal{F}(\Lambda^*/T^*, L/r_0) - 2\ln(\Lambda^*/T^*)]$, where $\mathcal{F}$ is

the function defined and tabulated by Phillips and Bruch (since F is an analytic function of A^*/T^* the values in their table are readily and accurately extrapolated to $A^*/T^* = 0$ by constructing a difference table). In this way we find, for T^* near 0,

$$A^* = -3.3710 + [1.17196 + \ln(2\pi)]T^* - T^* \ln T^* + O(T^{*2}). \tag{4}$$

Note that we will use throughout this paper the *configurational* Helmholtz free energy, defined by

$$A = -kT \ln\left[(1/N!) \int \cdots \int \exp(-V/kT)\, d\mathbf{r}_1 \ldots d\mathbf{r}_N\right], \tag{5}$$

where V is the potential energy, and the *configurational* internal energy defined using eqs. (5) and (2).

We fitted the MC data for the solid energy at $\rho^* = 0.9165$ in table III to the expression

$$U^* = -3.3710 + T^* - 0.3288T^{*2} + 0.2829T^{*3} - 0.1131T^{*4}. \tag{6}$$

The first term is the static lattice energy, the second is the equipartition value of the vibrational potential energy for two degrees of freedom, and the remaining three terms were determined from the MC data. This expression reproduces the MC data to within the statistical error (about ± 0.001). By combining (6) with the differential equation (2) and the boundary condition eq. (4) we find for the solid at $\rho^* = 0.9165$,

$$A^* = -3.3710 + 3.0098T^* - T^* \ln T^* + 0.3288T^{*2} - 0.1415T^{*3} + 0.0377T^{*4}. \tag{7}$$

For each of the temperatures, $T^* = 0.45, 0.55, 0.70, 1.00$, we calculated the free energy at $\rho^* = 0.9165$ from eq. (7) and the free energy at other densities by numerical integration of eq. (1) with intermediate pressures calculated by Lagrange interpolation of the MC data in table III.

For purposes of interpolation and integration we fitted the fluid phase pressure data to rational (Padé type) approximants of the form

$$\frac{p}{\rho kT} = \left(1 + \sum_1^5 f_i \rho^i\right) \Big/ \left(1 + \sum_1^4 g_j \rho^j\right), \tag{8}$$

with the coefficients given in table IV. The coefficients were determined to reproduce the correct second, third, fourth and fifth virial coefficients and to agree within the statistical uncertainty (about ± 0.02 in pV/NkT) with the MC data in table III for densities up to $\rho^* = 0.8$. Second, third and fourth virial coefficients are available in the literature[20,21]); fifth virial coefficients were taken from unpublished calculations by Barker[22]), and are listed in table IV.

TABLE III
Monte Carlo results

T^*	ρ^*	U^*	p^*	T^*	ρ^*	U^*	p^*
0.45	0.6	−1.952	−0.100				
0.45	0.7	−2.207	−0.044	0.45	0.7	−2.207	−0.04
0.45	0.739	−2.317	0.050	0.55	0.7	−2.120	0.23
0.45	0.75	−2.354	0.064	0.70	0.7	−2.050	0.71
				0.75	0.7	−2.025	0.92
0.55	0.3	−1.247	0.045	1.00	0.7	−1.928	1.67
0.55	0.5	−1.740	0.093				
				0.20	0.9165	−3.182	0.71
0.55	0.7	−2.120	0.231	0.40	0.9165	−3.007	2.28
0.55	0.79	−2.432	0.91	0.45	0.9165	−2.968	2.64
0.7	0.70	−2.050	0.71	0.55	0.9165	−2.884	3.38
0.7	0.75	−2.208	1.20	0.60	0.9165	−2.839	3.78
				0.70	0.9165	−2.763	4.45
0.7	0.80255	−2.367	2.01	0.80	0.9165	−2.683	5.15
0.7	0.82	−2.431	2.28	1.00	0.9165	−2.529	6.49
0.7	0.83	−2.466	2.45	0.45	0.82	−2.679	0.001
0.7	0.84	−2.513	2.53	0.45	0.87	−2.874	0.849
1.0	0.35	−0.990	0.32	0.55	0.846	−2.719	1.00
1.0	0.45	−1.243	0.47	0.55	0.87	−2.799	1.53
1.0	0.55	−1.500	0.70	0.70	0.87	−2.690	2.51
1.0	0.65	−1.779	1.26	0.70	0.90	−2.753	3.60
1.0	0.70	−1.928	1.67	0.70	0.855	−2.637	2.18
1.0	0.75	−2.065	2.39	1.00	0.94	−2.514	7.99
1.0	0.80	−2.178	3.51	1.00	0.882	−2.488	4.92

For $T = 1.0$ we calculated free energies by numerical integration according to the equation

$$A/NkT = \ln \rho^* - 1 + \int_0^{\rho^*} [p^*/\rho^{*2}T^* - 1/\rho^*]\, d\rho^* \tag{9}$$

with p^*/ρ^*T^* given by eq. (8). For the density $\rho^* = 0.7$ we fitted the liquid energies in table III to the expression

$$U^* = -2.3825 + 0.5346T^* - 0.08T^{*2} - 1.5259 \exp(-17T^{*2}) \tag{10}$$

again within the statistical uncertainty. We then used this expression with eq. (2) to calculate free energies at $\rho^* = 0.7$ and $T^* = 0.45$, 0.55 and 0.70. We used eqs. (8) and (1) to calculate free energies at other densities and chemical potentials from the equation

$$\mu^* = A^* + p^*/\rho^*. \tag{11}$$

Finally we determined the phase coexistence by solving the simultaneous

TABLE IV
Rational approximants for $p/\rho kT$ and fifth virial coefficients

T^*	0.45	0.55	0.70	1.0
f_1	−10.5045	−3.5966	−2.7141	−3.2086
f_2	20.7126	13.6709	16.2753	11.7969
f_3	−13.0723	−9.7282	−37.2291	−18.4305
f_4	2.5803	0.5640	36.7272	17.0168
f_5	0.0	0.0	0.0	0.0
g_1	−2.8466	1.2134	0.0464	−2.1356
g_2	10.9930	15.8445	12.0780	7.0799
g_3	−11.1515	9.6091	−14.2334	−5.9005
g_4	0.0	−40.0	0.0	0.0
E	186.26	−34.87	−55.28	−5.96

equations

$$\mu^*_{\text{fluid}} = \mu^*_{\text{solid}}, \tag{12}$$

$$p^*_{\text{fluid}} = p^*_{\text{solid}}. \tag{13}$$

This is equivalent to constructing common tangents to solid and fluid free energy/area curves (for the constant density calculations) or to locating crossings of μ^*/T^* curves (for constant pressure calculations); the latter case is, of course, somewhat simpler since eq. (12) is automatically satisfied.

The results are shown in table V, and in figs. 1 and 2. To produce the Monte Carlo curves in figs. 1 and 2 we carried out Lagrange interpolation of p^*, ρ^*_{fluid}, ρ^*_{solid} vs. T.

According to the results of Henderson[5]) the gas–liquid critical temperature is close to 0.55. Our Padé expression, eq. (8), for this temperature indicated that this temperature was slightly supercritical. We performed a short linear extrapolation in temperature using the Padé expressions for $T = 0.55$ and 0.70, and estimated the critical temperature $T^*_c = 0.526$. To avoid error from this extrapolation we performed MC calculations and constructed a Padé expression for $T^* = 0.526$, and used linear interpolation between 0.55 and

TABLE V
Fluid–solid transition data, Monte Carlo results

T^*	ρ^*_f	ρ^*_s	p^*	ΔH^*	ΔS^*
0.45	0.786	0.855	0.43	0.37	0.82
0.55	0.801	0.870	1.52	0.47	0.86
0.70	0.829	0.880	2.85	0.47	0.67
1.00	0.856	0.903	5.82	0.59	0.59

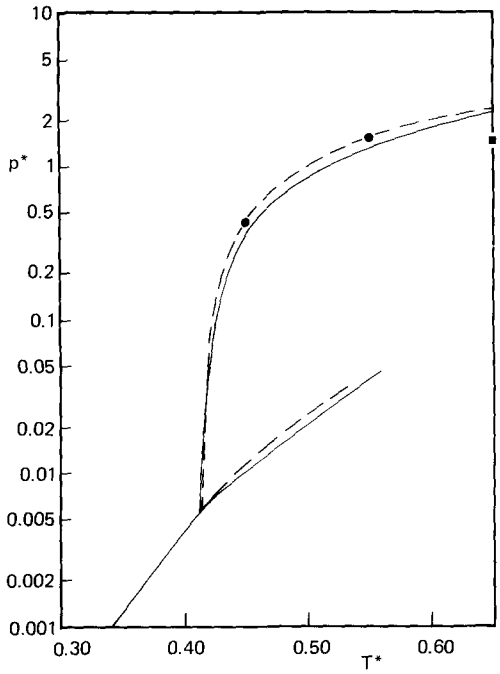

Fig. 1. Phase diagram in (T, p) plane. Solid lines, perturbation theory and self-consistent cell model. Dashed lines, Monte Carlo calculations (interpolated); circles are directly calculated values. The square indicates one of Toxvaerd's values.

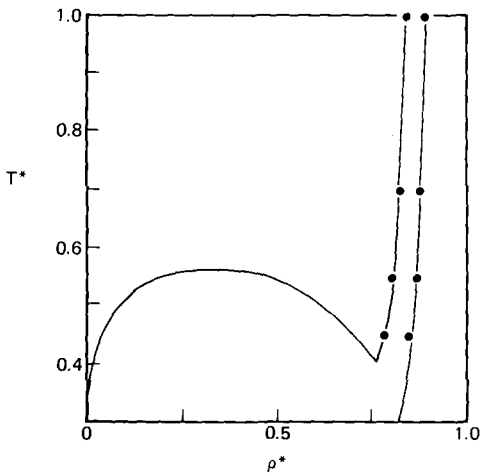

Fig. 2. Phase diagram in (ρ, T) plane. Solid lines, perturbation theory and self-consistent cell model. Circles, Monte Carlo results.

0.526 to estimate the critical parameters given in table I. Because the correct values of the second–fifth virial coefficients provide a strong constraint on the low-density part of the isotherm while the MC results control the high-density part we believe that these are fairly precise estimates.

Using our calculated free energies for the high-density fluid state at $T^* = 0.45$ and free energies calculated from eqs. (8) and (9) for the low-density fluid we calculated the vapor pressure of the liquid at $T^* = 0.45$. We also obtained in this way an estimate of the enthalpy of vaporization at $T^* = 0.45$. From the enthalpy of vaporization we calculated dp^*_{vap}/dT^* at $T^* = 0.45$. Using the three pieces of information (p^*_{vap} and dp^*_{vap}/dT^* at $T^* = 0.45$ and $p^*_{vap} = p^*_c$ at $T^* = T^*_c$) we determined constants for the Antoine equation,

$$\ln p^* = a - b/(c + T^*) \tag{14}$$

with $a = 1.4233$, $b = 1.9730$, and $c = -0.1150$, and this equation was used to construct the liquid–vapor equilibrium line shown as the dashed line in fig. 1.

To check whether our use of the constraint method of Hansen and Verlet[18]) was necessary to prevent liquid–gas phase separation we made a further calculation for $T^* = 0.45$ and $\rho^* = 0.60$. The system had been equilibrated with the constraint and the pressure stabilized at -0.1. We took the final configuration of this run as an initial configuration and ran for 2.4×10^6 configuration. The particle trajectories for this run are shown in fig. 4, and demonstrate clearly the existence of a gas "bubble", while the pressure averaged over the last 0.7×10^6 configurations was -0.01 (zero within statistical uncertainty). This behavior was also seen by Toxvaerd[4]) using molecular dynamics.

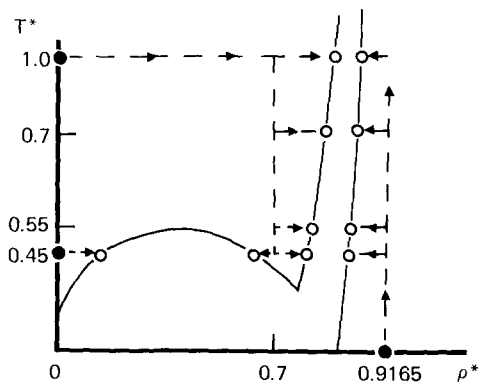

Fig. 3. Integration paths in (ρ, T) plane for calculating free energy. Solid circles represent initial states, open circles final states.

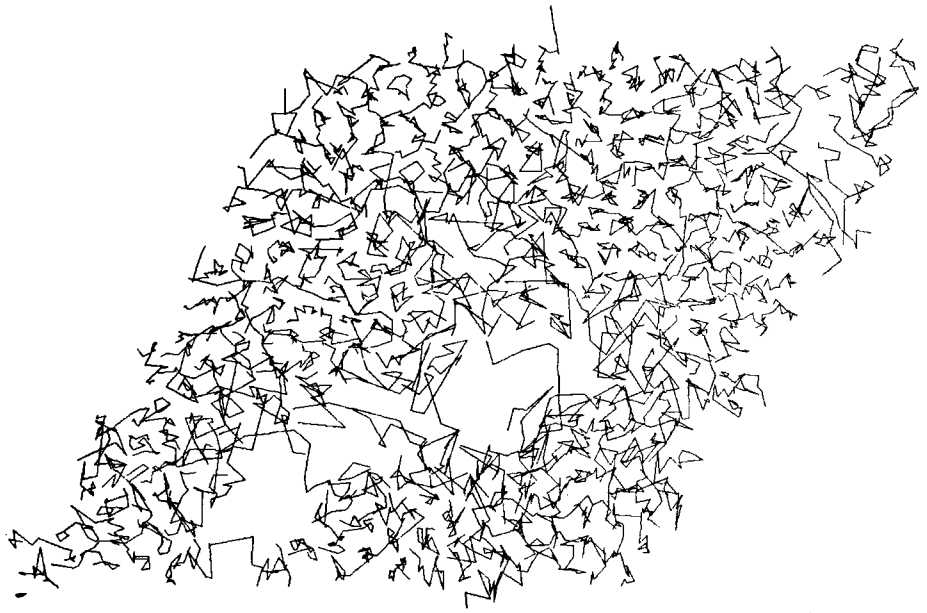

Fig. 4. Particle trajectories in MC simulation for $T^* = 0.45$, $\rho^* = 0.6$ without Hansen–Verlet constraint.

4. Discussion

The agreement between the phase diagram calculated from perturbation theory and that from the MC results is really quite striking. In fig. 5 we present, for the temperature $T^* = 0.7$, a comparison of the pressure density isotherm as calculated by various methods with the direct Monte Carlo data. For the fluid phase the perturbation theory results agree very well with the rational approximant and direct MC results except for some deviations in a narrow density range above $\rho^* = 0.8$. The self-consistent cell model agrees very well with the MC results for the solid phase. The nonself-consistent (Lennard-Jones–Devonshire) cell model also agrees moderately well with the MC results; the major advantage of the self-consistent version is that it gives much better values for the entropy.

The MC point P in fig. 5 is clearly in the two-phase region. This is shown in fig. 6 which exhibits particle trajectories in the MC simulation, and shows clearly the existence of solid and fluid regions. Thus the pressure at the point P provides us with a "direct coexistence" estimate of the melting pressure, $p^* = 2.5$; this is to be compared with our estimate of 2.85 from the free-energy calculations. Van Swol et al.[8]) comment that the "direct coexis-

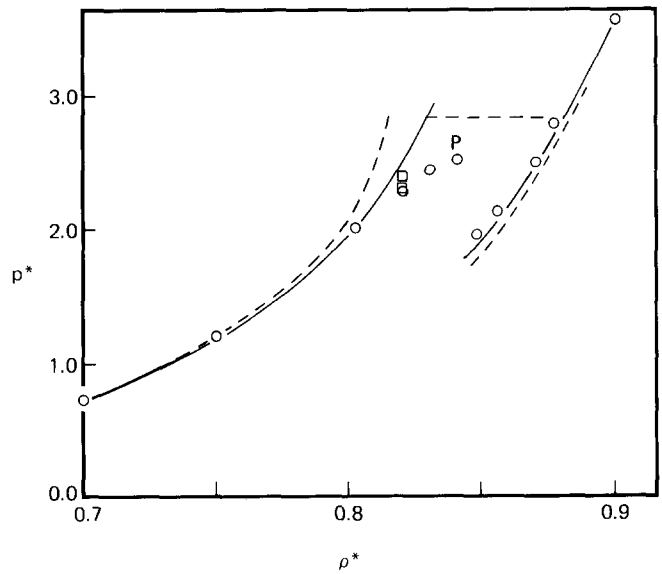

Fig. 5. Pressure density isotherm for $T^* = 0.7$. Circles and squares are constant density and constant pressure MC results, respectively. Dashed curve, $\rho^* < 0.82$ – fluid, perturbation theory, solid curve, $\rho^* < 0.82$ – fluid, rational approximant. Solid curve, $\rho^* > 0.82$ – solid, self-consistent cell model. Dashed curve, $\rho^* > 0.82$ – solid, Lennard-Jones and Devonshire cell model.

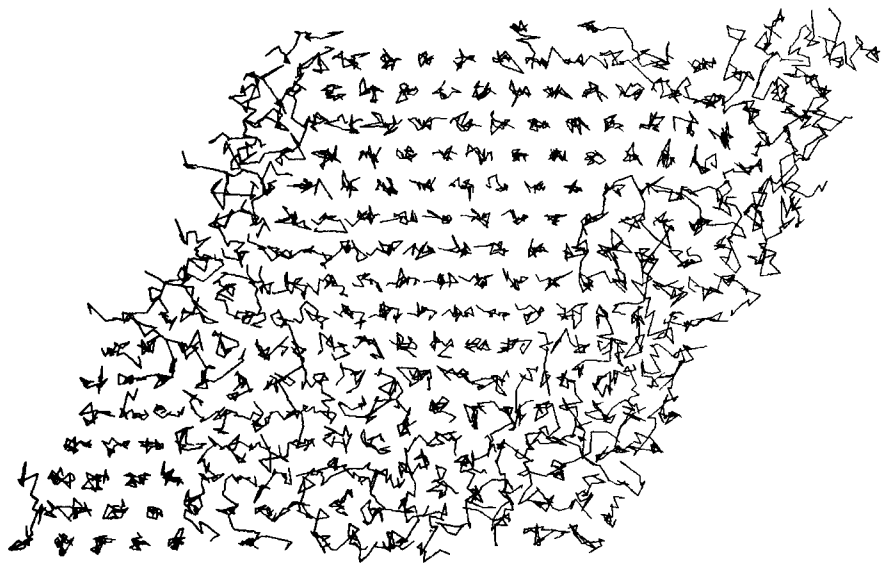

Fig. 6. Particle trajectories in two-phase region ($T^* = 0.7$, $\rho^* = 0.84$; point P in fig. 5).

tence" method would be expected to give a lower bound for the melting pressure, and they obtain a "direct coexistence" estimate for $T^* = 0.8$ of $p^* = 3.3$ which is also about 0.4 lower than our (interpolated) estimate from free energy calculations ($p = 3.7$).

Although our results are in qualitative agreement with those of Toxvaerd[3,4]) there are some quantitative deviations between his estimates of the phase boundaries[3]) and ours. His pressures and fluid and solid densities are substantially lower than ours (see fig. 2). Toxvaerd's pressures, for given fluid and solid densities, are consistent with ours, so that the source of the discrepancy must lie in the free energies, probably for the solid phase. To agree with Toxvaerd's results we would have to reduce our solid free energies by about 0.1, whereas we estimate the errors in our values as certainly less than 0.005. Toxvaerd used the "single-occupancy" method of Hoover and Ree[24]) to integrate the solid free energy. This has a problem with a second-order phase transition, and this could perhaps explain the discrepancy, as van Swol et al.[8]) suggested. The "loop" in fig. 5 is presumably a "small system" loop of the kind discussed by Hill[23]), which would vanish in the limit of large systems. Quantitative understanding of the behavior in the two-phase region would require a detailed analysis of the role of heterophase fluctuations and surface free energies in small systems, which we have not yet made.

Toxvaerd[4]) using molecular dynamics observed two-phase behavior like that shown in fig. 6, at $\rho^* = 0.8$, $T^* = 0.5$ (a point which lies well within our two-phase region), and commented that the six-fold anisotropy found by Frenkel and McTague[6]) is explained by the anisotropy in the solid co-existing phase. In this connection it is important to note that a "crystallite" in the two-phase region does not have time to rotate on the time-scale of the usual MC or molecular dynamics computation, so that as the crystallite moves by melting and freezing at the boundary it will retain a fixed orientation.

In conclusion we note that all of our results are consistent with the supposition that the phase diagram of the Lennard-Jones system in two dimensions is qualitatively similar to that in three dimensions, with first-order phase transitions separating solid, liquid and gaseous phases, and with a gas–liquid critical point. Earlier work of Abraham[7,8]) made a compelling case for this supposition, and we have discovered nothing which would tend to contradict it. The close agreement of our perturbation theory and cell model calculations with the "fluid" and "solid" branches of the isotherms tends to confirm the identification of those phases as ordinary fluid and solid phases. Our observation of solid and fluid regions in the two-phase region (fig. 5) suggests strongly that the six-fold anisotropy observed by Frenkel and McTague[6]) was due to ordinary solid–fluid coexistence rather than a "hexatic" phase, in agreement with Abraham[7,8]), Toxvaerd[4]), and Van Swol et al.[9]).

References

1) P.L. Fehder, J. Chem. Phys. **50** (1969) 2617.
2) F. Tsien and J.P. Valleau, Mol. Phys. **27** (1974) 177.
3) S. Toxvaerd, Mol. Phys. **29** (1975) 373; J. Chem. Phys. **69** (1978) 4750.
4) S. Toxvaerd, Phys. Rev. Letters **44** (1980) 1002.
5) D. Henderson, Mol. Phys. **34** (1977) 301.
6) D. Frenkel and J.P. McTague, Phys. Rev. Letters **42** (1979) 1632.
7) F.F. Abraham, Phys. Rev. Letters **44** (1980) 463.
8) F.F. Abraham, in Proc. Intern. Conf. on Ordering in Two Dimensions, S.K. Sinha, ed. (North-Holland, New York, 1980).
9) F. van Swol, L.V. Woodcock and J.N. Cape, preprint.
10) B.I. Halperin and D.R. Nelson, Phys. Rev. Letters **41** (1978) 121.
11) D.R. Nelson and B.I. Halperin, Phys. Rev. **B19** (1979) 2457.
12) B.J. Alder and T.E. Wainwright, Phys. Rev. **127** (1962) 359.
13) D. Henderson and J.A. Barker, Mol. Phys. **14** (1968) 587.
14) J.A. Barker and D. Henderson, J. Chem. Phys. **47** (1967) 4714.
15) J.A. Barker, J. Chem. Phys. **44** (1966) 4212.
16) J.A. Barker and E.R. Cowley, J. Chem. Phys. **73** (1980) 3452.
17) A. Bonissent, J.A. Barker and E.R. Cowley, in preparation.
18) J.P. Hansen and L. Verlet, Phys. Rev. **184** (1969) 151.
19) J.M. Phillips and L.W. Bruch, Surface Sci. **81** (1979) 109.
20) I.D. Morrison and S. Ross, Surface Sci. **39** (1973) 21.
21) E.D. Glandt, J. Chem. Phys. **68** (1978) 2952.
22) J.A. Barker, "Fifth Virial Coefficients for Lennard-Jones Fluid in Two Dimensions," to be published in Proc. Roy. Soc. (London).
23) T.L. Hill, "Thermodynamics of Small Systems" (Benjamin, New York, 1964).
24) W.G. Hoover and F.H. Ree, J. Chem. Phys. **49** (1968) 3609.